# A framework to Georeference Point Cloud in GPS Shadowed Urban Environment by Integrating Computer Vision Algorithms and Photogrammetric Techniques

Mayank Sharma[1,2,*], Raghavendra Sara[1] and Shefali Agrawal[1]
[1] Photogrammetry and Remote Sensing Department, Indian Institute of Remote Sensing, Dehradun, Uttarakhand
[2] Indian Institute of Technology Roorkee, Uttarakhand
*Email: mayanksharma.iirs@gmail.com

(Received: Jan 4, 2022; in final form Sep 13, 2022)

**Abstract**: The integration of computer vision algorithms and photogrammetric techniques has become an alternative to the high-cost Mobile Mapping Systems (MMS) and point cloud generation through Structure from Motion (SfM) algorithm is the best example of it. The point cloud generated using SfM is an arbitrary coordinate system and for its georeferencing known global coordinates of the camera exposure stations, rotational and translational parameters are required. The global coordinates of exposure stations are obtained through GNSS (Global Navigation Satellite System). GPS (Global Positioning System) is widely used for getting the positional information of a point. The problem in georeferencing the point cloud arises if the coordinates of a few camera exposure stations are unknown due to GPS shadowing or poor GDOP (Geometric Dilution of Precision). This issue is common in MMS that use laser scanners, GNSS and IMU (inertial measurement unit). In this paper, efforts are made to develop a methodology for handling GPS shadowing or poor accuracy for the georeferencing of arbitrary point clouds generated through SfM. The adopted method uses a blend of photogrammetric techniques of space resection and space intersection to determine the unknown camera exposure stations' coordinates. Bundle adjustment is applied to improve the accuracy of the results obtained. The developed methodology is well analyzed in different cases, and the results show good accuracy in respective cases.

**Keywords:** Computer Vision, space resection, space intersection, collinearity equations, GPS shadowing

## 1. Introduction

Computer vision and photogrammetry are different fields; however, their integration provides much easier 3D reconstruction from images. Computer vision algorithms are mathematical techniques for image-based reconstruction (Szeliski 2010). Computer vision algorithms are finding their applications both in photogrammetry and mobile mapping. The ability of computer vision algorithms to provide camera information (exterior orientation) has become an alternative to high-cost IMU (Inertial Measurement Unit)/INS (Inertial Navigation Sensors) and thus offer a cost-effective solution to high-cost Mobile Mapping technology for geospatial data collection with the rapid and easy acquisition of the data as the significant advantages (Li 1997).

The recent developments in digital photogrammetry and computer vision-based image processing techniques have formed a new milestone for image-based three-dimensional (3D) reconstruction (Mugnai and Tucci 2022). Both digital photogrammetry and computer vision are different fields, but their integration has numerous applications (Granshaw and Fraser 2015). The role of computer vision technology in Close range photogrammetric applications and mobile mapping technology is increasing at a high pace. Close range photogrammetry provides a low-cost solution for generating georeferenced 3D models, point cloud and digital elevation models (DEMs), etc., with good accuracy. A plethora of literature is available that reports good achievable accuracy through close-range photogrammetric applications. The integration of Computer Vision algorithms with photogrammetric processes is in high demand as this integration results in a cost-effective solution to mobile mapping systems (MMS).

A typical MMS consists of a mobile or moving platform, navigation, and mapping sensor. Mapping sensors may be metric and non-metric cameras, laser scanners, or RADARs. They are used for collecting information about the objects to be surveyed. Navigational sensors such as Global Positioning System (GPS)/IMU are used for obtaining positional and orientation information of the mapping sensors (Li 1997). Navigational sensors play a vital role in geocoding the data acquired from camera and Laser scanners. However, these sensors are expensive, due to which the MMS has been a costly geospatial mapping tool (Warnasch and Killen 2002). Despite this, IMU accumulates bias with time if not corrected by coupling it with GPS. Further, GPS unavailability or lower accuracy of GPS signals affect MMS working in GPS shadowed environments. GPS shadowed environments are the regions where GPS signals are not available or the satellite visibility is poor (Spilker 1996). Thus, Computer vision algorithms, along with photogrammetric techniques, are in high demand. The most widely used computer vision algorithm for point cloud generation is the structure from motion (SfM). It is used for image-based reconstruction and generates a point cloud in an arbitrary coordinate system. The integration of SfM with the photogrammetric techniques enables the estimation of camera parameters and generation of point clouds with reasonable accuracy (Yang et al. 2013). Further, if the coordinates of exposure stations are known, then the point cloud's georeferencing can be done using the direct georeferencing approach, in which the ground control points (GCPs) are not required (Gabrlik 2015; Rizaldy and Firdaus 2012). However, the unavailability or poor GDOP (Geometric Dilution of Precision) of GPS signal affects the point cloud's georeferencing accuracy (Liu et al. 2022). The possible reasons for GPS unavailability or poor accuracy are poor GDOP, high-rise buildings in urban areas and dense forest canopy, etc. Both photogrammetric and mobile mapping

technologies suffer from GNSS (Global Navigation Satellite System) signal unavailability and poor accuracy in GNSS shadowed regions.

This paper introduces an approach to handle the problem of GPS unavailability or lower accuracy in the GNSS shadowed regions for the georeferencing of an arbitrary point cloud generated using SfM. OSM (Open Street Map) Bundler software is a free software that works on SfM. The OSM Bundler software (Lourakis and Argyros 2009; Snavely et al. 2006, 2008) uses the Structure from Motion algorithm for the point cloud generation. PMVS (Furukawa and Ponce 2010) and CMVS packages are also available with Bundler to convert sparse point cloud to dense point cloud. The generated point cloud is in a local coordinate system. To georeference it, global coordinates of each camera exposure station are required. The technique to georeferenced the point cloud with the help of camera station coordinates is known as direct georeferencing. It does not require ground control points (GCPs) on the surface or target (Liu et al. 2022). Again, the requirement of GNSS availability with proper accuracy is mandatory to achieve better georeferencing accuracy.

## 2. Related works

Highly advanced real-time kinematic (RTK) GNSS receivers used in MMS are available nowadays. These RTK receivers are also used in drones or UAVs (Unmanned Aerial Vehicles) and capture the location of the camera exposure station. Although the accuracy of these instruments is high; however, the speed of drones in aerial surveys and vehicles' high speed in MMS may distort the positional accuracy of these instruments (Liu et al. 2022; Sanz-Ablanedo et al. 2018). Several researchers have highlighted that the accuracy of GNSS receivers plays a crucial role in the accurate georeferencing of the acquired datasets (McMahon et al., 2021). This study also focusses on the georeferencing accuracy of the point cloud data generated using SfM. SfM is a widely used algorithm for photogrammetric point cloud generation and is now more common in UAV photogrammetric processing (Martínez-Carricondo et al. 2018). However, the direct georeferencing of the products of SfM becomes challenging in case the accurate GPS locations of the camera exposure stations are unavailable or inaccurate.

A lot of work has already been done to improve GPS accuracy and handle GNSS unavailability. The capabilities of GPS receivers have already improved a lot to provide better accuracy in complex environments. Specific models are also developed to address the unavailability of GPS signals in dense urban and forest areas. Most of the studies to handle GNSS unavailability are in the field of intelligent driverless transportation. Architecture based on the integration of GNSS/INS instruments to update the position of a vehicle in the absence of GNSS signals is used by (Li et al. 2022). Hassan et al. (2006) present the photogrammetric approach to georeference the overlapping sequence of images captured through MMS in the absence of GPS signals or if weak signals are available. Even the proposed method produces good results; however, the use of VISAT MMS makes it an expensive approach because of its complex setup and high-cost instruments. Scarmana (2007) also explains developing a prototype to support mobile mapping in GPS unavailable areas using photogrammetric concepts, land surveying, and dead-reckoning techniques. Digital compass, laser range finder, and smartphone supporting GPS are used to configure a portable unit. Thus it requires several external instruments, which again becomes an expensive approach. Choi and Chang (2019) also used these external instruments (IMU and GPS) for accurately estimating the vehicular position in the shadowed regions. Their simulative study provided good accuracy in the shadowed areas. One of the studies presented by Nguyen et al. (2019) combines two range-based non-GPS localization methods by assigning different weights and performing the analysis of the combinations. The simulative study uses AOA (Angle of Arrival) and RSSI (Received Signal Strength Indicator) with different weights to analyze the effects of shadowing. It shows that accuracy and precision have significantly improved by increasing and decreasing the weight of AOA and RSSI, respectively.

The problem of GPS unavailability or poor performance of GPS receivers is commonly seen in dense urban areas and is well explained by Groves (2011). High-rise buildings in urban areas interrupt the proper reception of GPS signals and thus act as an obstruction for obtaining the appropriate positioning information in dense urban areas. Groves (2011) also explains the limitation of GPS in cross-street positioning and presents a shadow matching technique to achieve accurate positioning information in dense urban areas. In this technique, 3D city models are used to predict the availability of GPS signals. GPS, along with other GNSS satellites, is modelled to enhance signal availability in narrow streets or urban areas with high-rise buildings. Clark and Bevly (2008) presented a GPS/INS integrated approach to detect the signal attenuation and boost the GPS positioning accuracy in a shadowed environment. Several high-quality GPS receivers are also developed that support the efficient reception of weak GPS signals. Huang et al. (2009) explain the implementation of chaotic oscillators to enhance weak GPS signal reception. The application of non-linear dynamics has resulted in less acquisition time.

Images acquired from different static locations covering an object with proper successive overlap were used by Jariwala et al. (2014) to generate the three-dimensional point cloud by applying the SfM algorithm. Georeferencing of the generated three-dimensional point cloud was done using the space intersection technique. For georeferencing the generated point cloud, exposure station coordinates corresponding to the images used for point cloud generation are required and are obtained through DGPS (Differential GPS) survey. Thus, the impact of GPS unavailability or poor accuracy directly affects the georeferencing accuracy of the generated point cloud. Computer vision algorithms are widely used for image-based 3D reconstruction. Yang et al. (2013) used the SfM algorithm, Clustering Views for Multi-view Stereo (CMVS), Patch-based Multi-view Stereo (PMVS) and Poisson surface reconstruction techniques for 3D generation from the images taken from conventional

cameras. The benefit of using a computer vision algorithm (SfM) of not requiring any prior information of the camera's internal and exterior orientation parameters is highlighted in this study (Arévalo-Verjel et al. 2022). The research works highlighted in this section clearly indicate the need to handle the problem of GNSS shadowing and thus help boost the potential of this study.

### 2.1 Collinearity equations

As per the collinearity equations, the camera exposure station, an object point, and its image point in a 3D space lie along a straight line (DeWitt and Wolf 2000). Collinearity equations for space intersection are used to determine the coordinates of the unknown camera stations, and then bundle adjustment is applied to improve the results and achieve high accuracy. This approach can be utilized in Mobile Mapping Systems to overcome GPS unavailability or GPS shadowing. Figure 1 describes the existence of the collinearity condition among camera exposure station, object point on the ground, and its image point. This basic principle is utilized in the space intersection technique to determine an unknown camera station's coordinate.

To determine global coordinates of the points that are available on two or more overlapping images, interior and exterior orientation parameters are required. These orientation parameters are obtained using the Structure from Motion algorithm.

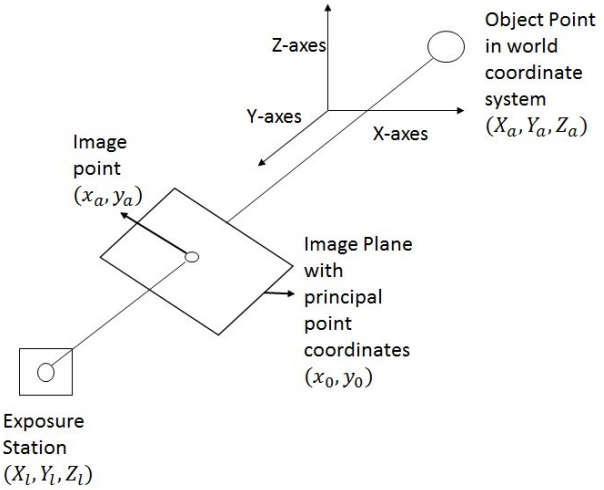


**Figure 1. Illustration of Collinearity Equation**

The collinearity conditions are generally expressed as:

$$x_a = x_0 - f * \left[\frac{m_{11}(X_A - X_L) + m_{12}(Z_A - Z_L) + m_{13}(Y_L - Y_A)}{m_{31}(X_A - X_L) + m_{32}(Z_A - Z_L) + m_{33}(Y_L - Y_A)}\right] \quad (1)$$

$$y_a = y_0 - f * \left[\frac{m_{21}(X_A - X_L) + m_{22}(Z_A - Z_L) + m_{23}(Y_L - Y_A)}{m_{31}(X_A - X_L) + m_{32}(Z_A - Z_L) + m_{33}(Y_L - Y_A)}\right] \quad (2)$$

Here, $(x_a, y_a)$ are image coordinates of the object points, $(x_0, y_0)$ are the principal point locations, $f$ is the focal length of the camera, $X_L, Y_L, Z_L$ are exposure station coordinates, $(X_A, Y_A, Z_A)$ are ground control points, $(m_{11}, m_{12} \ldots m_{33})$ are rotation parameters and are the functions of rotation angles (omega, phi, and kappa). The principal point location and focal length of the camera are intrinsic camera parameters. These parameters can be obtained by performing camera calibration. These camera parameters are required to handle the positional shift of a projected point onto an image plane (Scarmana, 2007).

## 3. Study area and dataset

The study area to conduct this study includes two buildings. The description of the selected buildings is given below:

Building 1: The first building chosen for this study is the main building of IIRS (Indian Institute of Remote Sensing), Dehradun, Uttarakhand. It has a simple architecture. Figure 2(a) shows the structure of Building 1.
Building 2: The second building chosen to validate the developed methodology is the building of the Godavari Hostel of IIRS, Dehradun, Uttarakhand. This building has comparatively complex architecture. Figure 2(b) shows the structure of Building 2.

The dataset used in this study includes the images acquired through the NIKON D60 camera without any zoom. The global coordinates of the image acquisition locations were measured along with the images, using the Trimble R7 GNSS (Global Navigation Satellite System) receivers. The GNSS data was post-processed in the Trimble Business Centre (TBC) software.


**Figure 2. (a) Building 1 and (b) Building 2**

## 4. Methodology for handling GNSS shadowed regions

The framework to carry out this study starts with the data collection task. The overlapped images of the study area are acquired sequentially using NIKON D60 camera mounted over a tripod. A total of 19 images are captured to cover the complete building façade. Along with image acquisition, the position of the camera exposure station is also measured using the Trimble R7 GNSS receiver. The global coordinates of the camera exposure station are required to georeferenced the point cloud data. To avoid the issue of time synchronization among sensors, the study is carried out in static conditions. The coordinates of camera exposure stations are obtained by the post-processing of DGPS data in Trimble Business Centre software. The developed methodology is tested on Building 1. In this case, the location of a few camera exposure stations assumed to be unknown, as shown in Figure 3. Thus, it requires that the unknown locations of camera exposure stations should be determined for georeferencing the point cloud generated from images using the SfM technique. The methodology to handle the GPS unavailability problem is shown in Figure 4. The images captured using the digital camera are processed

using OSM Bundler software (Snavely et al. 2006, 2008) to generate the sparse point cloud. Bundler uses the SfM computer vision algorithm for 3D sparse reconstruction. SfM is a highly robust computer vision algorithm that generates the sparse point cloud from overlapping images. It is the robustness of SfM that makes it suitable to apply it on disordered images.

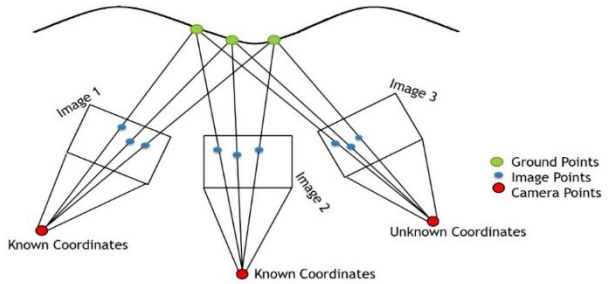


**Figure 3. GPS unavailability problem**

The point cloud generation through SfM include SIFT (Scale Invariant Feature Transform), ANN (Approximate Nearest Neighbour) (Mount and Arya 2010), RANSAC (Random Sample Consensus) algorithm (Fischler and Bolles 1981) and SBA (Sparse Bundle Adjustment) (Lourakis and Argyros 2009). The SIFT algorithm was developed by (Lowe, 1999) and is used for detecting the features in an image and matching them on other images using the Euclidean distance measurement. SIFT is a robust algorithm, independent of the image scale and orientation. It localizes the detected features and preserves their orientation information obtained through gradient analysis. In SIFT, multiple views are generated using the Gaussian scale space function as shown in equation (3) (Lowe 2004).

$$L(x, y, \sigma) = G(x, y, \sigma) * I(x, y) \quad (3)$$

Here * is representing the convolution of variable Gaussian scaling function ($G(x, y, \sigma)$) and the input image ($I(x, y)$). As given in equation (4), the DoG (Difference of Gaussian) method where the difference of two images are taken is implemented for getting the extrema of scale space.

$$D(x, y, \sigma) = L(x, y, k\sigma) - L(x, y, \sigma) \quad (4)$$

In equation (4), $D(x, y, \sigma)$ represents the difference between a scaled image and its unscaled version. To detect the stable features on the difference image ($D(x, y, \sigma)$), extremas are found by identifying the local maxima and minima by comparing every pixel to its 26 neighbours, in which eight neighbours belong to the same scale image and nine each in upscaled and downscaled images. Then, to remove the insignificant features, localizing the keypoints is done by computing the Laplacian on the difference images. It is computed by taking the second derivative of the difference image as given in equation (5). In this process, keypoints having poor contrast or are present on the edges are removed (Lowe 2004).

$$z = -\frac{\partial^2 D^{-1}}{\partial x^2} \frac{\partial D}{\partial x} \quad (5)$$

The value of $z$ signifies the stability of a key point. A key point is discarded, if its value is below a given threshold as it is considered to be the keypoint with lower contrast. A Hessian Matrix of order 2x2 is formed for the location of the keypoint. The ratio of this matrix's highest and lowest eigen vectors is compared to the curvature difference in the horizontal and vertical direction on the difference image. This comparison results in the removal of the keypoints present on the edges. Further, the selected keypoints are assigned an orientation. This orientation assignment ot the keypoints makes the algorithm orientation independent. Magnitude gradient and the orientation angles are estimated on the Gaussian smoothened image as per equations (6) and (7).

$$m(x, y) = \sqrt{(L(x+1, y) - L(x-1, y))^2 + (L(x, y+1) - L(x, y-1))^2} \quad (6)$$

$$\theta(x, y) = \tan^{-1}\left(\frac{(L(x,y+1) - L(x,y-1))}{(L(x+1,y) - L(x-1,y))}\right) \quad (7)$$

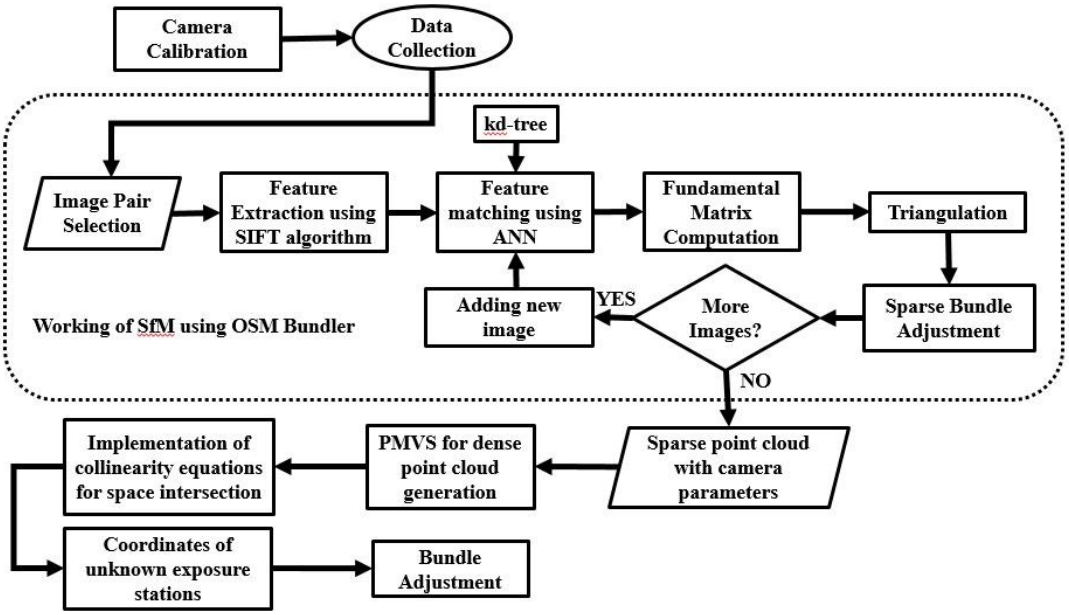


**Figure 4. Approach to handle GPS unavailability**

Estimated gradient of the orientation is then used to construct a histogram of orientation. The global maxima of the peaks in the histogram is used along with the other local maxima with height up to 80% of the highest peak, to assign the orientation to a keypoint. After orientation assignment, the image gradient data is further used for the creation of keypoint descriptors. The rotation in gradient data is made to align it with the keypoint's orientation and further assigned a weight by Gaussian window. The generated output is subsequently utilized for creating histograms with keypoint at the centre. The keypoint descriptors are arranged in grids of order 4x4. Each grid cell has a further 8 bin orientation histogram representing major directions as per the compass and their midpoints. This generated an output vector which is known as SIFT keys. Each feature vector or SIFT key contains 128 elements. These feature vectors or SIFT keys are further used for the feature matching task. For feature matching, firstly the SIFT feature descriptors are computed for an image and the corresponding SIFT keys are stored in a database. These feature vectors or SIFT keys are matched with the feature vectors of a new image. The matching depends on the Euclidean distance estimation among the feature vectors (Lowe 1999; Lowe 2004). The task of feature matching consumes a lot of time. Thus, ANN is used to optimize the feature matching process by identifying the closest neighbours. It uses kd-tree which is generated with every keypoints of an image (Mount and Arya 2010) so that any queried point could be easily matched with the keypoints of the other image. It uses Minkowski metrics that comprises of Manhattan, Euclidean and max distance. Feature matching also results in a few outliers, and removal of these outliers is necessary. RANSAC is used here to remove the outliers. RANSAC, an iterative algorithm, implements the least squares method to identify the outliers present in the dataset. Then the fundamental matrix is computed that preserves the information about the epipolar geometry and keep a track of relationship of matched feature points. The best matched image pairs are identified through fundamental matrix and a new image is taken further to find the matches again. Finally, the bundle adjustment is applied for parameters optimization and reconstruction of the sparse point cloud.

Along with the point cloud, Bundler generates a camera parameter file that contains the interior and exterior orientation parameters of each exposure station. These parameters are further used to solve the collinearity equations. Before data acquisition, the camera's intrinsic parameters like focal length, principal point location, and lens distortion parameters are estimated by performing camera calibration. To obtain the coordinates of an unknown camera station, global coordinates of at least two common points on the adjacent image (whose camera station coordinates are known) are required. These consecutive images should have proper overlap so that a single point is visible in at most two images. Since the coordinates of the exposure station of the adjacent image are known, so, the global coordinates of the common points can be calculated using collinearity equations. In this case, there are three unknowns $(X_A, Y_A, Z_A)$ so at least three equations are required to solve these equations. Since a point is available in at least two images, so four equations are obtained for a point (two from each image). Then the least square adjustment is applied to obtain the solution. Further to obtain the global coordinates of the unknown exposure station are calculated by using these known points as GCPs to solve equations 1 and 2. In this case, the unknowns are$(X_l, Y_l, Z_l)$. Therefore, two points are sufficient to obtain the solution of collinearity equations. Here more number of common points can increase the accuracy; however, two points are enough to get the solution of collinearity equations. A code to determine the coordinates of an unknown camera station is developed in Matlab as well as in Python for the implementation of collinearity equations. These obtained coordinates are used as initial values to perform bundle adjustment in Leica Photogrammetry Suite (LPS) to improve the accuracy of the obtained results.

## 5. Results and discussion

To handle the GPS shadowing or poor accuracy problem, a methodology is developed and is analyzed in different cases based upon the no. of photographs as well as control points. Different cases investigated are listed in Table 1. A program is developed in Python as well as in MATLAB to determine the coordinates of an unknown camera station by implementing the collinearity equations. As mentioned previously, the coordinates of camera exposure stations are obtained by processing the GPS data in Trimble Business Centre software. The horizontal and vertical accuracies obtained in the post-processing of GPS data are 0.6 cm and 0.9 cm, respectively. As mentioned in the methodology, control points are taken from the images whose camera exposure station coordinates are known. More number of control points provides better results. For this study, two buildings are chosen, one for developing the framework and another to verify it. A total of 19 images of Building 1 were taken for this study. The results obtained for different cases are explained in the following sections:

### 5.1 Case 1

Out of 19 images, the location of the camera station corresponding to image number 8 is assumed to be unknown. Inputs used to solve the collinearity equations and obtained coordinates for image number 8 are shown in Table 2.

Figure 5 shows the georeferenced point cloud of Building 1 and Building 2. The locations of all 19 camera exposure stations are shown in Figure 6.

An error of 12.65 m, 11.12 m and 9.54 m in easting, northing and height are obtained by solving the collinearity equations with the help of only two control points. These two control points were taken from the left adjacent image. To improve the solution, triangulation and bundle adjustment were applied using the Leica Photogrammetric Suite (LPS) of Erdas Imagine. The coordinates obtained by solving the collinearity equations were taken as initial coordinates during triangulation in LPS. The obtained error in coordinates with a different number of GCPs used in triangulation is shown in Table 3. The ground control points that are listed in the table are those points that were

used to adjust the block in LPS. From Table 3, it is clear that bundle adjustment improves accuracy and also with more ground control points accuracy improves. It is also clear that with 30 ground control points, errors in easting, northing and height are 3.01 m, 3.98 m and 2.07 m, respectively. This shows that with more GCPs, the accuracy improves. However, there is no significant change in the accuracy.

The collinearity equations are again solved with six control points and corresponding errors in easting, northing and height are obtained as 2.73 m, 2.98 m, and 2.12 m. In this case, three control points were taken from the left image and the other three from the right image adjacent to the image whose exposure station coordinates are unknown. After processing the block in LPS, the error obtained in the coordinates of the unknown camera station were 0.86 m, 0.92 m, and 0.81 m respectively in easting, northing and height with 25 GCPs. It was found that the control point locations used for solving the collinearity equations play a significant role in the calculation of unknown camera exposure station coordinates. In case 1a, two almost collinear points were used and the error obtained was significant, whereas, in case 3 control points on adjacent images were well distributed and the error obtained was comparatively much less.

**Table 1. Description of different cases used for analysis**

| Cases | Number of images | No. of unknown camera stations | No. of control points used for solving collinearity equations |
|---|---|---|---|
| 1a | 19 | 1 | 2 |
| 1b | 19 | 1 | 6 |
| 2a | 4 | 1 (Last image) | 6 |
| 2b | 4 | 1(3rd image) | 6 |
| 2c | 4 | 2 | 6 |

**Table 2. Inputs used to solve collinearity equations and obtained coordinates of unknown camera station**

| | |
|---|---|
| Image coordinates of two points used (mm) | $\begin{bmatrix} 534.2467 & -239.4600 \\ -318.0120 & -239.7760 \end{bmatrix}$ |
| Principal Point coordinates (mm) | $[11.930593 \quad 8.037962]$ |
| Rotation Parameters (rad) | $\begin{bmatrix} 0.9957 & 0.0768 & 0.0520 \\ -0.0747 & 0.9964 & -0.0396 \\ -0.0548 & 0.0355 & 0.9979 \end{bmatrix}$ |
| GCPs (m) | $\begin{bmatrix} 215814.288539 & 3360261.242831 & 655.161734 \\ 215814.032010 & 3360262.015736 & 655.103009 \end{bmatrix}$ |
| Calculated coordinates of exposure station (m) | $\begin{bmatrix} 215804.785031 \\ 3360262.42872 \\ 654.86307229 \end{bmatrix}$ |

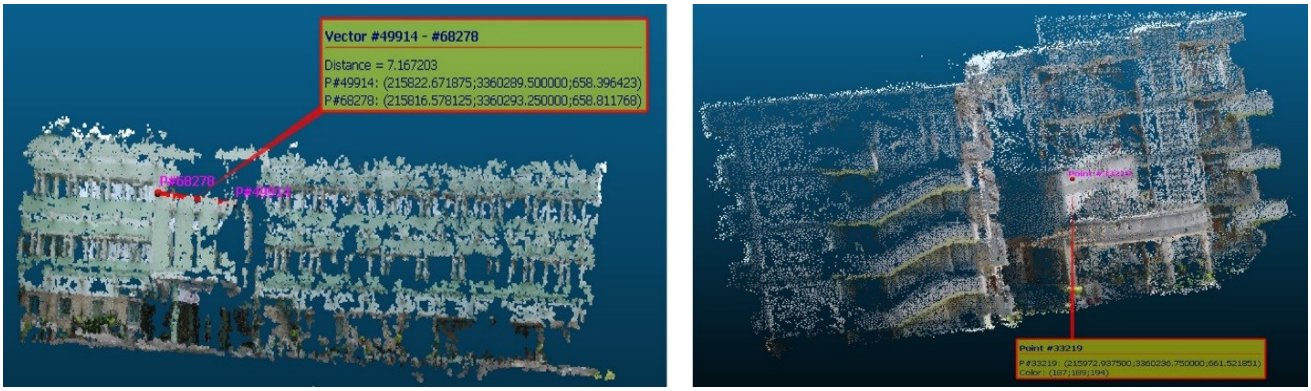


**Figure 5. Georeferenced point cloud of Building 1 and Building 2**

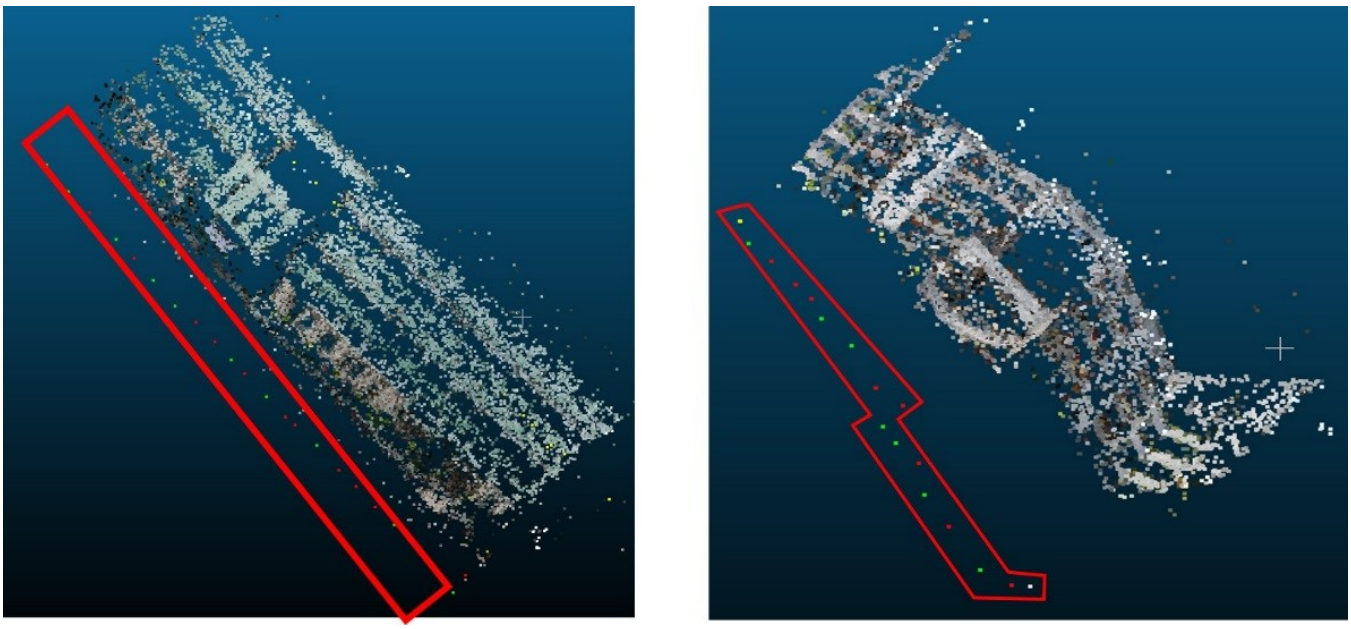

**Figure 6. Location of camera exposure stations Building 1 (left) and Building 2 (right)**

**Table 3. Error in Coordinates**

| No. of Ground Control Points | Frame No. | Easting(m) | Northing(m) | Height(m) |
|---|---|---|---|---|
| 25 | 8 | 3.25 | 4.66 | 2.18 |
| 30 | 8 | 3.01 | 3.98 | 2.07 |

**5.2 Case 2**

The developed methodology is also analyzed by reducing the number of Images. This case is further divided into three subcases. In this case, the total number of control points used is six and a total of 4 images are taken.

*5.2.1 Case 2a*

Out of 4 images, the exposure station coordinates of last (4th) image frame are assumed as unknown. Error in Easting, Northing, and Height is shown in Table 4.

**Table 4. Error in coordinates of the 4th frame**

| Frame No. | Easting(m) | Northing(m) | Height(m) |
|---|---|---|---|
| 4 | 0.90 | 1.65 | 1.19 |

*5.2.2 Case 2b*

Now, the approach is applied when the coordinates of a middle camera station (3rd image frame) are unknown. Here, it is assumed that the third camera station is unknown, and the obtained error is shown in Table 5.

**Table 5. Error in coordinates of the 3rd image frame**

| Frame No. | Easting(m) | Northing(m) | Height(m) |
|---|---|---|---|
| 3 | 0.91 | 0.99 | 0.50 |

It is clear from Table 5 that the accuracy improves if the coordinates of the adjacent (left and right both) camera stations are known.

*5.2.3 Case 2c*

Considering the case when the coordinates of the two camera stations are unknown. It is assumed that the coordinates of the third and fourth camera stations are unknown. The error obtained in the coordinates of the 3rd and 4th camera stations is shown in Table 6.

**Table 6. Error in coordinates of 3rd and 4th camera station**

| Frame No. | Easting(m) | Northing(m) | Height(m) |
|---|---|---|---|
| 3 | 0.84 | 1.95 | 0.50 |
| 4 | 1.14 | 2.24 | 1.72 |

It is clear from Table 6 that as the number of unknown camera stations increases, the accuracy reduces. The error in the coordinates of the fourth camera station indicates that the error increases if the adjacent camera stations are unknown.

The developed methodology is verified on the captured images of Building 2. The developed framework works well and produces similar results.

## 6. Conclusions

Even highly efficient MMS suffers from the tracing through GNSS shadowed regions and handling such constraints becomes essential to build up a low-cost MMS. The methodology developed in this research work to address GPS unavailability problems for the georeferencing of an arbitrary point cloud generated using SfM is well analyzed in different cases. It provides a cost-effective solution to handle GPS unavailability in shadowed regions. A collinearity-based solution is suggested treating the global transformed local points as GCPs for obtaining the position of an unknown camera station. Various cases analyzed in this research show that

more distributed GCPs improve the estimation of locations by performing bundle adjustment. The error increases if a large number of consecutive camera stations are unknown. Known adjacent camera stations produce good results. This study integrates computer vision algorithms and photogrammetric-based approaches to handle GPS unavailability in shadowed areas. It can be utilized in MMS and to supplement IMU corrections.

**Acknowledgment**

We thank the Director, Indian Institute of Remote Sensing, Dehradun, for providing us with the necessary hardware and infrastructure to conduct this study.

**References**

Arévalo-Verjel A. N., J. L. Lerma, J. F. Prieto, J. P. Carbonell-Rivera and J. Fernández (2022). Estimation of the Block Adjustment Error in UAV Photogrammetric Flights in Flat Areas. Remote Sensing 2022, Vol. 14, Page 2877, 14(12), 2877. https://doi.org/10.3390/RS14122877

Choi E. and S. Chang (2019). An Adaptive Tracking Estimator for Robust Vehicular Localization in Shadowing Areas. IEEE Access, 7, 42436–42444. https://doi.org/10.1109/ACCESS.2019.2907647

Clark B. J. and D. M. Bevly (2008). GPS/INS integration with fault detection and exclusion in shadowed environments. In Record - IEEE PLANS, Position Location and Navigation Symposium (pp. 1–8). https://doi.org/10.1109/PLANS.2008.4569963

DeWitt B. A. and P. R. Wolf (2000). Elements of Photogrammetry(with Applications in GIS) (3rd ed.). New York: McGraw-Hill Higher Education.

Fischler M. A. and R. C. Bolles (1981). Random sample consensus: a paradigm for model fitting with applications to image analysis and automated cartography. Communications of the ACM, 24(6), 381–395. https://doi.org/10.1145/358669.358692

Furukawa Y. and J. Ponce (2010). Accurate, dense, and robust multiview stereopsis. IEEE transactions on pattern analysis and machine intelligence, 32(8), 1362–1376.

Gabrlik P. (2015). The use of direct georeferencing in aerial photogrammetry with micro UAV. IFAC-PapersOnLine, 28(4), 380–385. https://doi.org/10.1016/j.ifacol.2015.07.064

Granshaw S. I. and C. S. Fraser (2015). Editorial: Computer Vision and Photogrammetry: Interaction or Introspection? The Photogrammetric Record, 30(149), 3–7. https://doi.org/10.1111/phor.12092

Groves P. (2011). Shadow Matching: A New GNSS Positioning Technique for Urban Canyons, 417–430. https://doi.org/10.1017/S0373463311000087

Hassan T., C. Ellum and N. El-Sheimy (2006). Bridging land-based mobile mapping using photogrammetric adjustments. In Proceedings of the ISPRS Commission I Symposium ‘‘From Sensors to Imagery. Citeseer.

Huang P., Y. Pi and Z. Zhao (2009). Weak GPS signal acquisition algorithm based on chaotic oscillator. Eurasip Journal on Advances in Signal Processing, 2009. https://doi.org/10.1155/2009/862618

Jariwala J. J., A. Bhardwaj, S. Raghavendra, and K. Khoshelham (2014). Feasibility of Mobile Mapping System by Integrating Structure from Motion(SfM) approach with Global Navigation Satellite System. In Proceedings of AGSE 2013: The Geospatial Momentum for Society and Environment (Vol. 6, pp. 116–132).

Li B., G. Chen, Y. Si, X. Zhou, P. Li, P. Li and T. Fadiji (2022). GNSS/INS Integration Based on Machine Learning LightGBM Model for Vehicle Navigation. Applied Sciences 2022, Vol. 12, Page 5565, 12(11), 5565. https://doi.org/10.3390/APP12115565

Li R. (1997). Mobile mapping: An emerging technology for spatial data acquisition. Photogrammetric Engineering and Remote Sensing, 63(9), 1085–1092.

Liu X., X. Lian, W. Yang, F. Wang,Y. Han and Y. Zhang (2022). Accuracy Assessment of a UAV Direct Georeferencing Method and Impact of the Configuration of Ground Control Points. Drones 2022, Vol. 6, Page 30, 6(2), 30. https://doi.org/10.3390/DRONES6020030

Lourakis M. I. A. and A. A. Argyros (2009). SBA: A software package for generic sparse bundle adjustment. ACM Transactions on Mathematical Software, 36(1), 1–30. https://doi.org/10.1145/1486525.1486527

Lowe D. G. (1999). Object Recognition fromLocal Scale-Invariant Features. IEEE International Conference on Computer Vision.

Lowe D. G. (2004). Distinctive Image Features from Scale-Invariant Keypoints. International Journal of Computer Vision 2004 60:2, 60, 91–110. https://doi.org/10.1023/B:VISI.0000029664.99615.94

Martínez-Carricondo P., F. Agüera-Vega, F. Carvajal-Ramírez, F. J. Mesas-Carrascosa, A. García-Ferrer and F. J. Pérez-Porras (2018). Assessment of UAV-photogrammetric mapping accuracy based on variation of ground control points. International Journal of Applied Earth Observation and Geoinformation, 72, 1–10. https://doi.org/10.1016/J.JAG.2018.05.015

McMahon C., O. E. Mora and M. J. Starek (2021). Evaluating the Performance of sUAS Photogrammetry with PPK Positioning for Infrastructure Mapping. Drones 2021, Vol. 5, Page 50, 5(2), 50. https://doi.org/10.3390/DRONES5020050

Mount D. M. and S. Arya (2010, January 27). ANN - Approximate Nearest Neighbor Library. http://www.cs.umd.edu/~mount/ANN/. Accessed 5 August 2022

Mugnai F. and G. Tucci (2022). A Comparative Analysis of Unmanned Aircraft Systems in Low Altitude Photogrammetric Surveys. Remote Sensing 2022, 4(3), 726.

Nguyen N. M., L. C. Tran, F. Safaei, S. L. Phung, P. Vial, N. Huynh., et al. (2019). Performance evaluation of non-GPS based localization techniques under shadowing

effects. Sensors (Switzerland), 19(11), 1–21. https://doi.org/10.3390/s19112633

Rizaldy A. and W. Firdaus (2012). Direct georeferencing: A new standard in photogrammetry for high accuracy mapping. In International Archives of the Photogrammetry, Remote Sensing and Spatial Information Sciences - ISPRS Archives (Vol. 39, pp. 5–9). https://doi.org/10.5194/isprsarchives-XXXIX-B1-5-2012

Sanz-Ablanedo E., J. H. Chandler, J. R. Rodríguez-Pérez and C. Ordóñez (2018). Accuracy of Unmanned Aerial Vehicle (UAV) and SfM Photogrammetry Survey as a Function of the Number and Location of Ground Control Points Used. Remote Sensing 2018, Vol. 10, Page 1606, 10(10), 1606. https://doi.org/10.3390/RS10101606

Scarmana G. (2007). Mobile mapping in gps-denied areas: a hybrid prototype. In A. Vettore & N. El-Sheimy (Eds.), The 5th International Symposium on Mobile Mapping Technology. Padua, Italy.

Snavely N., S. M. Seitz and R. Szeliski (2006). Photo tourism: exploring photo collections in 3D. In ACM transactions on graphics (TOG) (Vol. 25, pp. 835–846). ACM.

Snavely N., S. M. Seitz and R. Szeliski (2008). Modeling the World from Internet Photo Collections. International Journal of Computer Vision, 80(2), 189–210. https://doi.org/10.1007/s11263-007-0107-3

Spilker J. J. J. (1996). Foliage Attenuation For Land Mobile Users. In Global Positioning System: Theory and Applications, Volume I (pp. 569–583). American Institute of Aeronautics and Astronautics. https://doi.org/doi:10.2514/5.9781600866388.0569.0583

Szeliski R. (2010). Computer vision: algorithms and applications. Springer Science & Business Media.

Warnasch A. and A. Killen (2002). Low cost, high G, micro electro-mechanical systems (MEMS), inertial measurements unit (IMU) program. Position Location and Navigation Symposium, 2002 IEEE. https://doi.org/10.1109/PLANS.2002.998922

Yang M.-D., C.F. Chao, K. S. Huang, L. Y. Lu and Y. P. Chen (2013). Image-based 3D scene reconstruction and exploration in augmented reality. Automation in Construction, 33, 48–60. https://doi.org/10.1016/j.autcon.2012.09.017